J Mol Model (2007) 13:839–849
DOI 10.1007/s00894-007-0192-9

ORIGINAL PAPER

Non-empirical study of the phosphorylation reaction catalyzed by 4-methyl-5-β-hydroxyethylthiazole kinase: relevance of the theory of intermolecular interactions

Edyta Dyguda-Kazimierowicz · W. Andrzej Sokalski · Jerzy Leszczyński

Received: 20 December 2006 / Accepted: 27 February 2007 / Published online: 24 March 2007

Abstract The subject of this study was an analysis of the role of active site residues in the phosphoryl transfer reaction catalyzed by 4-methyl-5-β-hydroxyethylthiazole kinase (ThiK). The ThiK-catalyzed reaction is of special interest due to the lack of a highly conserved aspartate residue serving as a catalytic base. ONIOM(B3LYP:PM3) models of stationary points along the reaction pathway consisted of reactants, two magnesium ions and several highly conserved ThiK active site residues. The results indicate that an S_N2-like mechanism of ThiK, with γ-phosphate acting as an alcohol-activating base is reasonable. Geometries of substrates, transition state and products were utilized in the non-empirical analysis of the physical nature of catalytic interactions taking place in the ThiK active site. The role of particular residues was investigated in terms of their ability to preferentially stabilize the transition state relative to substrates (differential transition state stabilization, DTSS) or products (differential product stabilization, DPS). It seems that Mg2, Glu126 and Cys198 play a major catalytic role, whereas Mg1 and the same Cys198 are responsible for product release. It is remarkable that no dominant role of an electrostatic term in the interactions involved in catalytic activity is observed for product release. Determination of catalytic fields expressing differential electrostatic potential of the transition state with respect to substrates revealed the optimal electrostatic features of an ideal catalyst for the studied reaction. The predicted catalytic environment is in agreement with experimental data showing increased catalytic activity of ThiK upon mutation of Cys198 to aspartate.

Keywords Catalytic fields · Enzymatic catalysis · Interaction energy · Phosphoryl transfer · Ribokinase-like kinases

E. Dyguda-Kazimierowicz (✉) · W. A. Sokalski
Department of Chemistry, Wrocław University of Technology,
Wyb.Wyspiańskiego 27,
50-370 Wrocław, Poland
e-mail: edyta.dyguda@pwr.wroc.pl

W. A. Sokalski
e-mail: andrzej.sokalski@pwr.wroc.pl

J. Leszczyński
Jackson State University,
Jackson, MS, USA

Introduction

The great interest in the catalytic properties of kinases originates from their participation in multiple metabolic and regulatory pathways. Despite facilitating essentially the same phoshoryl transfer reaction, kinases exhibit remarkable diversity in their structure and substrate specificity [1]. The latter implies either that the same (or similar) reaction can be accomplished in several ways or that analogous catalytic mechanisms are achieved with the involvement of different active site residues that together exhibit some common characteristics.

The most extensively studied kinases are protein kinases transferring a terminal phosphate group from ATP to protein substrates [2]. On the other hand, small molecule kinases, such as those representing the ribokinase superfamily [3], are much less frequently investigated and little is known about the molecular basis of their catalytic activity. To fill this gap and to allow comparisons with the current view of kinase action, we focused on the catalytic mechanism of the phosphoryl transfer reaction performed by 4-methyl-5-β-hydroxyethylthiazole kinase [4] (Thz kinase, ThiK). ThiK is a member of the ribokinase family of sugar kinases that phosphorylate substrates containing a

hydroxymethyl group. ThiK-catalyzed phosphorylation of the thiazole moiety constitutes a salvage branch in the biosynthetic pathway of thiamine. Despite significant similarity to other ribokinase-like kinases (e.g., ribokinase [5], adenosine kinase [6], pyridoxal kinase [7]), ThiK lacks the highly conserved aspartate residue (replaced by Cys198) otherwise believed to serve as a catalytic base during the phosphorylation process. Surprisingly, a cysteine to aspartate mutation results in a ninefold increase in ThiK enzymatic activity [4]. Other features of the ThiK active site, including the presence of magnesium ion(s), a positive helix dipole and an oxyanion hole, as well as the overall positioning of ligands within existing X-ray structures, are consistent with an S_N2-like mechanism comprising a direct nucleophilic attack of a substrate hydroxyl group oxygen on the γ-phosphorus of ATP [8]. Nevertheless, this hypothesis has been tested neither experimentally nor via theoretical modeling. Among the questions that remained unanswered is the actual number of magnesium ions required for catalysis as well as the role of Cys198 and Arg121 residues. The guanidinium moiety of the latter provides an additional electrostatic stabilization of β-phosphate—the interaction specific to Thz kinases.

The purpose of this study was to test the suggested pathway of ThiK-catalyzed phosphorylation of Thz and to determine the possible involvement in catalysis of specific ThiK active site components. By rigorous ab initio calculations of the interaction energy we evaluate the concept of differential transition state stabilization as well as the role of active site residues in product release. Furthermore, application of interaction energy decomposition enables determination of both the physical nature of binding and the residues that are crucial for catalytic activity. As a result, approximate, yet well-founded models can be constructed that can aid in prediction of the influence of enzyme mutations on enzymatic activity. Finally, catalytic fields methodology is employed in the development of qualitative characteristics of a catalyst optimal for a given reaction.

Methods

Computational method

The geometries of reactants, transition state and products were determined using the two-layered ONIOM(B3LYP/6-31G(d):PM3) approach [9–12] as implemented in the Gaussian 03 program [13]. The starting structure of reactants was extracted from previous molecular mechanics and semiempirical simulations [14]. The model reaction system was then simplified to include highly conserved residues (see Fig. 1) suggested to be important for catalysis (i.e., Asp94, Arg121, Glu126, and Cys198) as well as two magnesium ions together with their solvation spheres (water molecules Wat82, Wat112, Wat126, Wat567, and Wat575). The magnesium ion denoted as Mg1 interacts with oxygen atoms from β- and γ-phosphates and is coordinated to Wat112, Wat126, and Wat575. The two remaining water molecules, Wat82 and Wat567, are bound to Mg2 interacting with α- and β-phosphates. Both Asp94 and Glu126 participate in water-mediated coordination of Mg1.

The multiple sequence alignment of Thz kinases from several bacterial species shown in Fig. 1 indicates the ThiK residues used in this analysis as an active site model. The first sequence in this alignment (denoted as THIM_BACSU according to Swiss-Prot database [15] nomenclature) belongs to *Bacillus subtilis* ThiK, which is the subject of this study. As can be seen from Fig. 1, the four amino acid

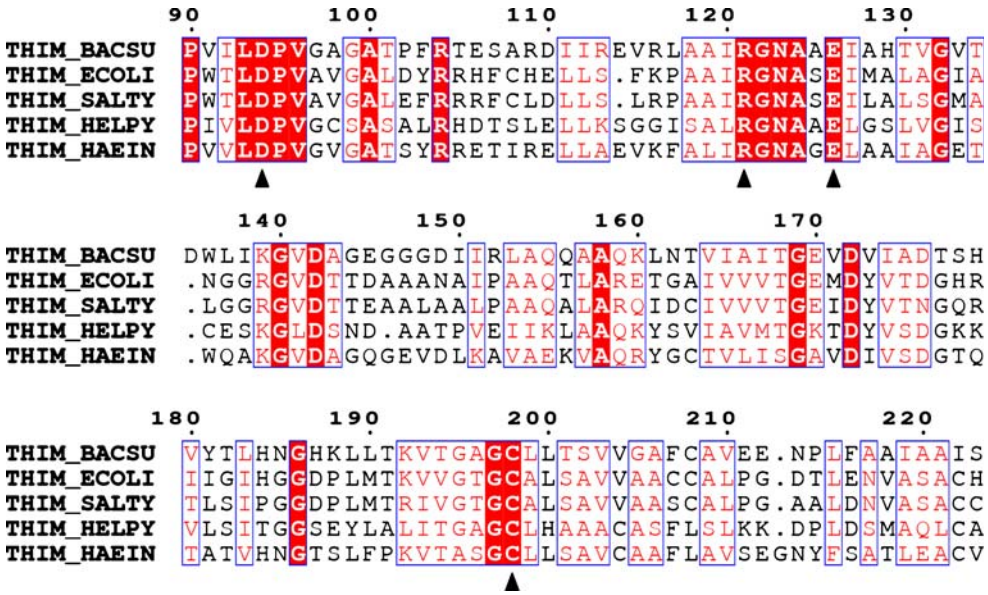

Fig. 1 Multiple sequence alignment of 4-methyl-5-β-hydroxyethylthiazole (Thz) kinases (THiK). *Blue boxes* indicate significant similarity (in terms of amino acid physical–chemical properties). *Red background* denotes identity. *Triangles* mark residues serving as a model active site in this study. Thz kinase sequences from the following species are shown: *Bacillus subtilis* (THIM_BACSU), *Escherichia coli* (THIM_ECOLI), *Salmonella typhimurium* (THIM_SALTY), *Helicobacter pylori* (THIM_HELPY), *Haemophilus influenzae* (THIM_HAEIN)

residues considered here are among the most highly conserved residues within the Thz kinase family. Sequence alignment was performed with CLUSTAL W [16] and printed using ESPript [17] tool.

To limit the size of the system, arginine and cysteine residues were represented by methylguanidinium cation and methanethiol, whereas an acetate molecule was used to mimic aspartate and glutamate side chains. The only neutral residue was then Cys198 (see explanation below), while carboxylic moieties as well as guanidinium group were assumed to be either negatively ($Asp94^{-}$, $Glu126^{-}$) or positively charged ($Arg121^{+}$). The protonation state of aspartate and glutamate was chosen as the most probable due to their involvement in coordination of the positively charged magnesium ion [4]. Similarly, the arginine residue has been attributed a role in stabilization of negatively charged phosphates [4] and thus is likely to be positively charged. ATP and Thz were modelled by methyl triphosphate and ethanol, respectively, and only these latter molecules were included in the region described by higher level theory. As suggested recently, the triphosphate moiety of ATP in aqueous solution is fully deprotonated under neutral conditions [18]. Due to the influence of the protein environment, there are numerous possible protonation states; however, a charge of −4 is generally accepted as the most likely, especially when the triphosphate tail is coordinated to two magnesium ions [19, 20]. Therefore, the methyl triphosphate considered herein was assumed to bear a charge of −4. The other substrate—ethanol—is unlikely to be deprotonated in the initial stages of reaction [4] and it was thus modelled as a neutral species.

Since a reliable verification of transition state relevance would not be possible in the case of a model containing fixed entities, all atoms in the system were allowed to move during optimization and the final complexes turned out to be stable. The change in substrate structure associated with the optimization procedure was measured by the RMS deviation (RMSD) of its heavy atoms calculated with respect to the starting complex. Relatively high RMSD values (i.e., 2.3 Å) could partially be explained by a possible errors in the reference structure itself (due to its molecular mechanics origin, [14]). RMSD corresponding to the displacement of heavy atoms from the reacting molecules (including magnesium ions) is significantly lower (i.e., 0.9 Å) indicating greater stability of the model core as opposed to increased mobility of the surrounding amino acid residues. Comparison with any experimental structure could not be performed due to the lack of data regarding ThiK–substrate complexes; crystal structures of Thz kinase are available only for Thz alone or the ATP/Thz-phosphate complex [4] (Protein Data Bank access codes of 1C3Q and 1ESQ, respectively). Moreover, the structure containing ATP and phosphorylated Thz corresponds to the Cys198Ser mutant. Nonetheless, the stability of final quantum mechanically derived structures can be used to support their reliability. The nature of particular stationary points found along the reaction coordinates as well as thermodynamic properties (zero point energy correction, enthalpies, and Gibbs free energies) were determined by vibrational frequency analysis.

Based on the structures of S/TS/P complexes with ThiK active site residues (magnesium ions were also considered as a part of the active site environment), the energies of interaction between those residues and the reacting molecules (i.e., ATP and Thz) were then evaluated in a pairwise manner and further partitioned to reveal the physical nature of active site interactions. Such an approach has already been proven to be extremely useful when applied to analysis of both catalytic [21] and inhibitory [22] activity of enzymes. According to the variation-perturbation procedure [23], total interaction energy at the second-order Moller–Plesset level of theory can be partitioned into the electrostatic ($E_{EL}^{(1)}$), exchange ($E_{EX}^{(1)}$), delocalization ($E_{DEL}^{(R)}$) and correlation ($E_{CORR}^{(R)}$) components:

$$E^{MP2} = E_{EL}^{(1)} + E_{EX}^{(1)} + E_{DEL}^{(R)} + E_{CORR}^{(R)}$$

A well-defined hierarchy of theoretical models characterized by gradually increasing accuracy and computational cost can be established, opening the way for a reasonable derivation and testing of approximate models:

$$E_{EL}^{(1)} < E^{(1)} < E^{SCF} < E^{MP2}$$

In the above equation, $E^{(1)}$ denotes the first-order Heitler–London term calculated as $E^{(1)} = E_{EL}^{(1)} + E_{EX}^{(1)}$. Noticeably, all terms listed above are evaluated using a dimer-centered basis set to account for basis set superposition error (BSSE) by means of a counterpoise correction scheme [24]. Interaction energy values presented in the following were calculated with the 6-31G(d) basis set using a modified version of the GAMESS-US program [25].

The catalytic activity of a given molecular environment originates from lowering of the activation energy barrier for a catalyzed reaction, and can also be analyzed in terms of differential transition state stabilization (DTSS) with respect to the substrates. Along with the DTSS approach [26], lowering of the reaction activation barrier (Δ_{DTSS}) is equivalent to the difference in strength of transition state (E_{TS}) versus reactants binding (E_S) with the catalytic environment:

$$\Delta_{DTSS} = E_{TS} - E_S$$

Thus, the stronger a given environment interacts with the transition state compared to the corresponding interaction with reactants, the lower is the resulting activation energy barrier and the faster the reaction proceeds.

Since an overall reaction rate also depends on the rate of product release, another issue one could consider is the strength of transition state binding in comparison with the product stabilization energy, i.e. differential product stabilization, $\Delta_{DPS,TS}$:

$$\Delta_{DPS,TS} = E_P - E_{TS}$$

Phosphorylation of alcohols is generally shown to have a favourable equilibrium constant [27]. However, in the case of the reversible $S \leftrightarrow P$ reaction, $\Delta_{DPS,TS}$ can be thought of as a parameter describing the ease of a reverse reaction, i.e. a positive value would indicate lowering of the activation barrier for the reverse reaction. Since the transition state is an extremely short-lived species, one could also point out the necessity of considering differential product stabilization with respect to substrates, $\Delta_{DPS,S}$:

$$\Delta_{DPS,S} = E_P - E_S$$

Thus, it can be interesting to compare the idea of a possible role of the differential effects of $\Delta_{DPS,TS}$ and $\Delta_{DPS,S}$ in the product release step.

Whenever the electrostatic term is dominant, an even more simplified approach can be applied to estimate the optimal catalytic environment for a given reaction. Since the difference in molecular electrostatic potential generated by transition state and reactants expresses the influence of a positive unit charge on activation barrier lowering, simply considering the so-called static catalytic field [26], $\Delta_S = -\left(V^{TS} - V^S\right)$, allows the most favourable distribution of charges within a hypothetical catalytic environment to be predicted.

To assess the importance of ThiK residues not included in the active site model considered here, the reactant and transition state structures were inserted into the starting molecular mechanics model of the Thik–substrate complex. Any possible bad contacts were removed by short minimization performed with the CHARMM program [28] (version 31) and all-hydrogen parameter set from the CHARMM27 force field [29]. Optimization was followed by evaluation of pairwise interaction energy between each residue located within a 10 Å cutoff around the reactant/transition state and the latter. Binding energy was expressed as the sum of electrostatic and van der Waals terms, as defined within the CHARMM27 force field. Since no additional parametrization was performed, transition state structure was described by the same set of atomic point charges as reactants. Apart from residues already included in the quantum mechanical model of the active site, three amino acid residues (i.e., Arg104, Asn123, and Gly197) were found to contribute more than 1 kcal mol^{-1} to differential transition state stabilization. Because the average distance between Arg104 and reactant/transition state is 6 Å, as well as its contribution to DTSS is rather insignificant (+1.3 kcal mol^{-1}), this residue seems to be of minor importance in the ThiK-catalyzed reaction. Similar characteristic in terms of preferential transition state binding is exhibited by Gly197 (+1.4 kcal mol^{-1}); however, the close distance (i.e., 1.8 Å) between its main chain amino group and the γ-phosphate oxygen might indicate that a more in-depth study should probably account for the presence of this residue. Finally, much higher contribution to DTSS (+8.00 kcal mol^{-1}) is provided by Asn123 interacting via its side-chain amino group with the β-phosphate oxygen atom (minimum distance of 2.5 Å in the ThiK–reactants complex). The magnitude of differential transition state destabilization arising from the Asn123 residue results from the significant rearrangement of its side chain when going from the reactant- to the transition state-complex. The corresponding minimum distance decreased from 2.5 Å to 2.0 Å. It is thus unclear whether this outcome should be considered as a conclusive result, since it might originate from the lack of transition state structure reparametrization. Due to the uncertain role of Asp123, further calculations should probably take this residue into account. Finally, it should be clearly stated that the CHARMM calculation was performed only to estimate the possible contribution to DTSS arising from ThiK residues neglected while building the ONIOM active site model, whereas the latter was utilized for the non-empirical analysis of interaction energy. As has been shown in our parallel study of urokinase inhibition [30], force field optimization tends to underestimate the distances between interacting species and, thus, the analysis of binding energy decomposition carried out herein was based on the quantum mechanically derived structures.

Results and discussion

Phosphoryl transfer reaction

The structures of the reactants, transition state and products for ThiK-catalyzed processes are presented in Fig. 2. In the present study, only the most probable reaction course, which consists of an S_N2-like nuclephilic substitution at the phosphorus atom [4], was modelled. When considering the cleavage of a phosphoester bond, the range of mechanisms, that can occur, is bound by two limiting cases, i.e. the mechanism is either fully dissociative or fully associative [31]. The dissociative pathway, analogous to the S_N1 reaction in organic chemistry, proceeds via a highly reactive trigonal metaphosphate intermediate. The corresponding distances between the oxygen atoms from a leaving/entering group and the phosphorus atom is greater than the respective sum of van der Waals radii (i.e., 3.3 Å). The fully associative mechanism involves a pentavalent bipyra-

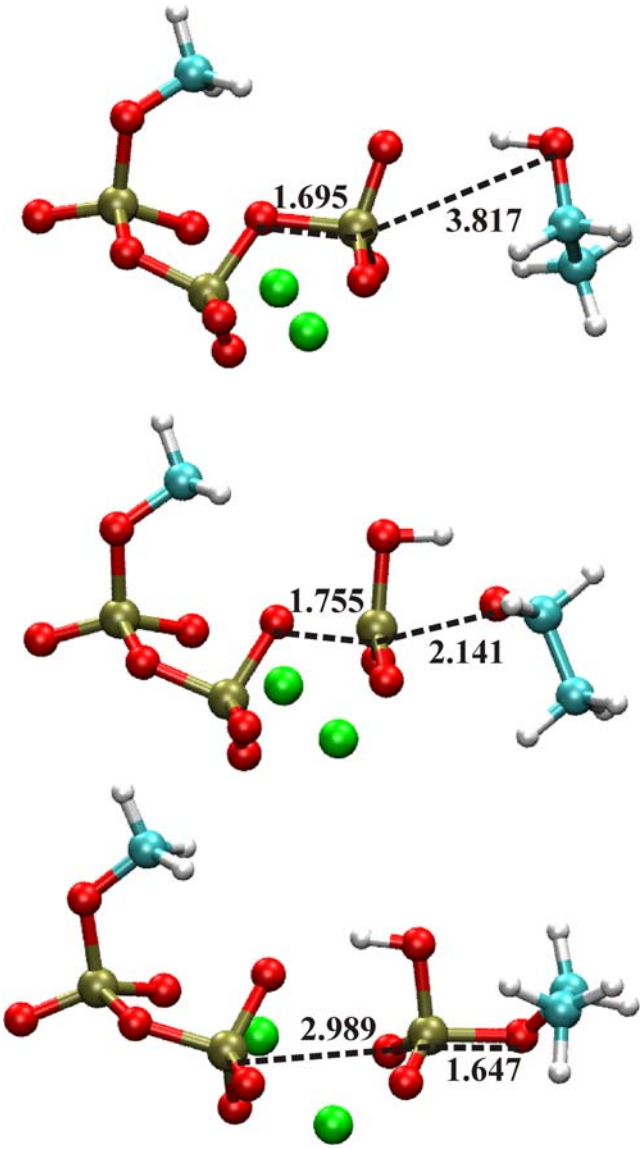

Fig. 2 B3LYP/6-31G(d):PM3 optimized geometries of reactants (*top*), transition state (*middle part of drawing*) and products (*bottom*). Only the reacting molecules (i.e., methyl triphosphate and ethanol representing ATP and Thz) and the two magnesium ions are shown. The crucial distances are denoted as *black dashed lines*

midal phosphorane intermediate with the length of the axial phosphorus–oxygen bonds (i.e., 1.73 Å) indicating their covalent character [31]. Between these two extremes are located intermediate cases described by partially associative S_N2-like mechanisms and the occurrence of a transition state with axial bonds lengths between 1.73 and 3.3 Å.

As mentioned above, kinase-catalyzed phosphorylation reactions often imply the involvement of an aspartate residue acting as an alcohol activating base. Its role consists of deprotonation of an attacking nucleophile prior to the actual formation of a phosphorus–oxygen bond. In case of Thz kinase, only the cysteine residue (Cys198) is present in the vicinity of the attacking hydroxyl group. Moreover, site-directed mutagenesis studies on Thik have suggested that the cysteine residue is not likely to be deprotonated during the phosphoryl transfer and, thus, it is not directly involved in catalysis (cysteine to alanine or serine mutants are only slightly less active) [4]. Presumably, the γ-phosphate oxygen atoms could also act as a catalytic base increasing the nucleophilicity of a substrate hydroxyl group and aiding in proton transfer during the reaction. The results of our simulation seem to confirm this suggestion—one of the γ-phosphate oxygen atoms is hydrogen bonded to a Thz hydroxyl moiety and its distance to the hydroxyl proton is equal to 2.05 Å.

Since no intermediates were found along the considered reaction coordinate, and a single transition state encompasses the trigonal bipyramidal geometry of a transferred phosphate, the overall phosphorylation pathway is consistent with an S_N2-like mechanism. According to the Pauling formula as proposed by Mildvan [31], the fractional bond number *n* providing a quantitative measure of associativity can be calculated based on the length of an axial bond to entering group in the model considered, *D(n)*, and the single phosphorus-oxygen bond distance, *D(1)*:

$$D(n) = D(1) - 0.60 \log (n)$$

Since *D(n)* and *D(1)* are equal to 2.14 and 1.73 Å, respectively, the discussed mechanism is 80% dissociative. A minor increase in the distance to the leaving group oxygen (1.76 compared to 1.70 Å) suggests the late departure of a phosphate donor. Notably, the expected proton transfer to the γ-phosphate oxygen atom occurs prior to transition state formation. However, the rather large activation energy barrier of ~40 kcal mol^{-1} (see Table 1) indicates that either a more realistic catalytic environment should be considered (i.e., a ThiK active site model consisting of a greater number of residues) or that an alternative reaction pathway associated with a lower energy barrier may exist.

Differential transition state stabilization

The next step in this study consisted of assessing the involvement in catalysis of each active site residue present in the model system. The putative catalytic role can be

Table 1 Relative energies (kcal mol^{-1}) of the transition state and product with respect to reactant structures as derived from B3LYP/6-31G(d):PM3 calculations. ΔE corresponds to the sum of electronic and zero-point energies, while ΔH and ΔG stand for the enthalpy and Gibbs free energy, respectively

	ΔE	ΔH	ΔG
Reactant	0.0	0.0	0.0
Transition state	40.2	38.7	44.4
Product	9.2	8.1	10.6

Table 2 Differential transition state stabilization (DTSS) energy (kcal mol^{-1}) at various levels of theory

Residue	$\Delta_{EL}^{(1)}$	$\Delta^{(1)}$	Δ^{SCF}	Δ^{MP2}
Glu126	−5.95	−5.94	−5.88	−5.44
Cys198	−5.13	1.39	−3.95	−5.30
Mg2	−3.30	−5.18	−4.53	−3.91
Wat112	−3.61	−2.25	−2.97	−3.02
Wat567	−0.35	−0.91	−0.85	−0.80
Wat82	0.21	−0.37	−0.28	−0.20
Wat575	−4.29	1.58	0.75	−0.12
Asp94	−0.16	−0.14	−0.30	0.19
Mg1	7.34	5.34	4.49	3.26
Wat126	7.19	3.86	4.32	4.12
Arg121	7.89	10.67	12.90	12.52
sum	−0.16	8.04	3.67	1.30
R[a]	0.88	0.89	0.99	1.00

[a] Correlation coefficient—applies to the relationship between results at a particular level of theory and MP2 results

analyzed within DTSS methodology allowing the most favourable (i.e., those increasing the reaction rate) residues to be recognized. In general, the greater the strength of interaction of a given residue with the transition state with respect to the substrates, the lower the activation energy barrier, resulting in a higher rate enhancement. Thus, such a residue can be considered as catalytically active, since its presence promotes catalysis.

Table 2 gives the results of interaction energy analysis expressed in terms of DTSS energy. The ordering of residues reflects their decreasing contribution to differential transition state stabilization. These results are also presented in Figs. 3 and 4. The most catalytically effective residues (i.e., those that bind the transition state stronger than the reactants) are Glu126, Cys198, and Mg2. Surprisingly, Arg121 seems to disfavor catalysis by stabilizing the substrates instead of the transition state and, due to its significant influence, the overall differential effect is slightly positive (total Δ^{MP2}=1.30 kcal mol^{-1}), indicating the actual lack of preferential transition state stabilization. This observation could suggest that it might be necessary to include the more complete active site representation in further calculation. However, one should keep in mind that the total interaction here is assumed to be equal to the sum of pairwise interactions and, thus, many body effects are neglected. Depending on the magnitude of these effects, the results of our present analysis are likely to be sensitive to the partitioning of a whole system into interacting species. Moreover, the treatment of magnesium ions and water molecules as entities separately interacting with transition state/reactants may be artificial, since these water molecules are first of all coordinated to their corresponding magnesium ions. Similarly, Arg121 was found to interact strongly with residue Asp94 (via two hydrogen bonds) suggesting a need for their simultaneous handling. To test this hypothesis, an analogous calculation was performed with water molecules treated as a part of particular magnesium ions clusters, and Asp94, Arg121 residues considered as a single moiety interacting with TS/S (Table 3).

The overall DTSS effect summarized in Table 3 is now negative (total Δ^{MP2}=−4.39 kcal mol^{-1}), denoting the stabilization of transition state relative to reactants. However, the magnitude of this stabilization is still not large.

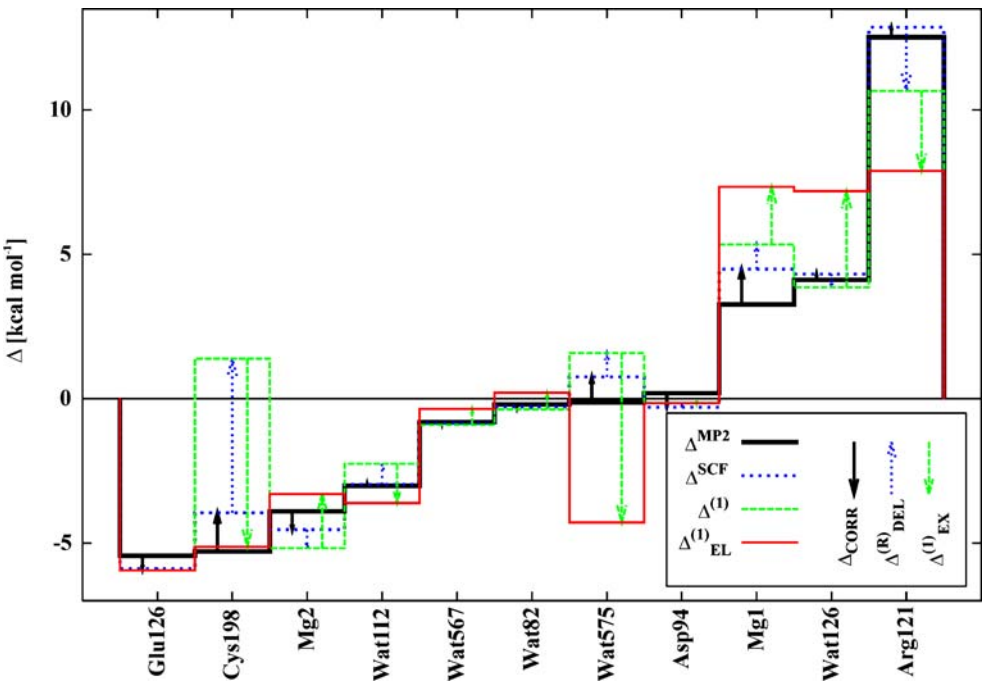

Fig. 3 The components of differential transition state stabilization (DTSS) energy (kcal mol^{-1}). For each residue, the transition state stabilization energy (relative to substrates) is given at subsequent levels of theory. *Vertical arrows* show the mutual cancellation of correlation, delocalization, and exchange corrections to the MP2 interaction energy

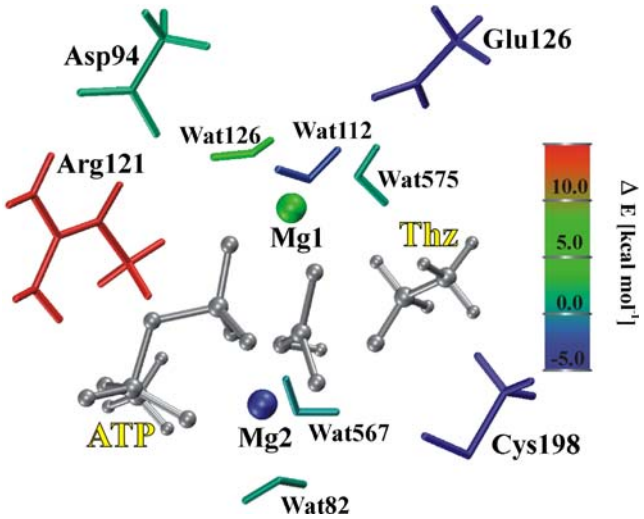

Fig. 4 Geometry of the complete transition state model. Active site residues (*stick representation*) are colored according to their contribution to differential transistion state stabilization (see energy scale on the right hand side)

Apparently, some other amino acid residues not considered here are also important for catalytic efficiency. As previously, the presence of Mg1 appears to have a slightly destabilizing effect on the transition state. This result is rather unexpected, since Mg1 is generally believed to increase the rate of catalyzed phosphoryl transfer, whereas an inhibitory influence has been attributed to Mg2 (as reported in case of protein kinase A, PKA [32]). However, similar results (i.e., greater contribution of Mg2 to transition state stabilization) were obtained in a QM/MM simulation of PKA-catalyzed phosphoryl transfer [20]. Finally, the total destabilizing effect of Asp94, Arg121 residues is smaller than the sum of pairwise interactions, indicating that many-body contributions also play a role in the overall interaction energy.

Considering the accuracy of consecutive levels of theory applied to the description of interactions, analysis of correlation with the most precise results at MP2 level demonstrates very good agreement between corresponding interaction energy terms (Tables 2, 3). In particular, correlation effects seem to be of minor importance in the case analyzed (the correlation coefficient of SCF results with respect to those at MP2 level is 0.99). Moreover, neglecting delocalization and exchange effects is also justified—the corresponding correlation coefficients are 0.89 and 0.88, respectively. As can be seen in Fig. 3, subsequent corrections to binding energy tend to cancel each other out to a remarkable degree. Nonetheless, systematic improvement is obtained by application of higher level of theory in the description of interactions.

Table 3 DTSS energy (kcal mol^{-1}) at various levels of theory. Magnesium ions together with water molecules comprising their solvation sphere were considered as single residues. Similar treatment was also employed in case of Asp94, Arg121 residues

Residue	$\Delta_{EL}^{(1)}$	$\Delta^{(1)}$	Δ^{SCF}	Δ^{MP2}
Mg2:Wat	−3.54	−6.81	−6.24	−5.65
Glu126	−5.95	−5.94	−5.88	−5.44
Cys198	−5.13	1.39	−3.95	−5.30
Mg1:Wat	6.35	7.36	4.66	1.76
Asp94:Arg121	5.33	8.38	10.41	10.24
sum	−2.94	4.38	−1.00	−4.39
R[a]	0.86	0.84	0.98	1.00

[a] Correlation coefficient—applies to the relationship between results at a particular level of theory and MP2 results

Differential product stabilization

To account for the effect of product release on the overall reaction rate, the concept of DTSS has been extended to the description of influence of a given residue on the product departure step. Accordingly, stabilization of products relative to the transition state (equivalent to differential product stabilization, $\Delta_{DPS,TS}$) can be associated with the reverse reaction. Similarly, product stabilization with respect to substrate, $\Delta_{DPS,S}$, should also impede product departure, especially bearing in mind the rapid transition state dynamics. Obviously, residues destabilizing the products with respect to either the transition state or substrates would facilitate product release. Nevertheless, this approach should be applied with some care, since the effects studied here cannot be attributed directly to a single well-defined property.

The results of DPS,TS analysis are presented in Tables 4 and 5 and Fig. 5. As previously, in addition to separate treatment of magnesium ions and water molecules, as well as Asp94 and Arg121 residues (Table 4, Fig. 5), their

Table 4 Differential product stabilization with respect to transition state (DPS,TS) energy (kcal mol^{-1}) at various levels of theory

Residue	$\Delta_{EL}^{(1)}$	$\Delta^{(1)}$	Δ^{SCF}	Δ^{MP2}
Mg1	−10.94	−10.62	−11.67	−12.11
Arg121	−10.36	−10.07	−11.77	−11.50
Wat82	−19.34	−3.87	−8.77	−8.90
Wat567	−3.48	−7.21	−7.76	−7.12
Mg2	5.78	−15.94	−0.93	−1.20
Wat126	−0.20	1.46	0.75	0.73
Asp94	1.90	1.91	1.83	1.18
Glu126	1.97	1.97	1.70	1.39
Wat112	3.34	1.02	1.41	1.44
Wat575	−17.58	13.91	8.08	7.16
Cys198	5.52	1.50	7.22	8.37
Sum	−43.40	−25.95	−19.91	−20.46
R[a]	0.45	0.72	1.00	1.00

[a] Correlation coefficient—applies to the relationship between results at a particular level of theory and MP2 results

Table 5 DPS,TS energy (kcal mol^{-1}) at various levels of theory. Magnesium ions together with water molecules comprising their solvation sphere were considered as single residues. Similar treatment was also employed in case of Asp94, Arg121 residues

Residue	$\Delta_{EL}^{(1)}$	$\Delta^{(1)}$	Δ^{SCF}	Δ^{MP2}
Mg2:Wat	−18.42	−31.18	−25.92	−26.02
Asp94:Arg121	−6.31	−6.02	−7.79	−7.70
Glu126	1.97	1.97	1.70	1.39
Mg1:Wat	−23.82	9.63	4.84	5.54
Cys198	5.52	1.50	7.22	8.37
Sum	−41.06	−24.10	−19.96	−18.42
R[a]	0.42	0.96	1.00	1.00

[a] Correlation coefficient—applies to the relationship between results at a particular level of theory and MP2 results

Table 6 Differential product stabilization with respect to substrate (DPS,S) energy (kcal mol^{-1}) at various levels of theory

Residue	$\Delta_{EL}^{(1)}$	$\Delta^{(1)}$	Δ^{SCF}	Δ^{MP2}
Wat82	−19.13	−4.24	−9.05	−9.10
Mg1	−3.60	−5.27	−7.18	−8.85
Wat567	−3.84	−8.12	−8.60	−7.92
Mg2	2.48	−21.12	−5.47	−5.00
Glu126	−3.98	−3.97	−4.19	−4.06
Wat112	−0.27	−1.25	−1.56	−1.58
Arg121	−2.47	0.60	1.10	1.03
Asp94	1.74	1.77	1.54	1.37
Cys198	0.39	2.89	3.27	3.07
Wat126	6.99	5.32	5.07	4.85
Wat575	−21.86	15.49	8.84	7.04
Sum	−43.55	−17.91	−16.25	−19.16
R[a]	0.09	0.76	0.99	1.00

[a] Correlation coefficient—applies to the relationship between results at a particular level of theory and MP2 results

simultaneous interaction as magnesium–water or Asp94: Arg121 clusters is also considered (Table 5). According to the definition, residues exhibiting positive DPS,TS values destabilize the product and promote its release. Notably, the arrangement of residues according to increasing differential product stabilization (i.e., the inverse of the order applied in Tables 4 and 5) is essentially the same as that obtained in the case of the DTSS study. The residue contributing the highest preferential product destabilization with respect to transition state is Cys198. The absolute amount of DPS,TS attributable to Arg121 is almost equivalent to DTSS—both reactants and products are stabilized more strongly than the transition state. The possible role of magnesium ions remains similar only when they are considered separately from water molecules. Once the interaction with solvated magnesium ions is taken into account (Table 5), Mg1 exhibits higher affinity to the transition state, facilitating product release. This result could provide an explanation for the differing roles of the two magnesium ions. Specifically, Mg2 appears to be important for catalytic activity due to its contribution to DTSS, while Mg1 could possibly enhance product departure by binding the transition state preferentially compared to products.

Results of a similar analysis performed according to DPS,S scheme (Tables 6, 7, Fig. 6) bear a close resemblance to those already found in the case of DPS,TS differential effects. The main difference is the inverse effect of residue Arg121, which appears to slightly destabilize

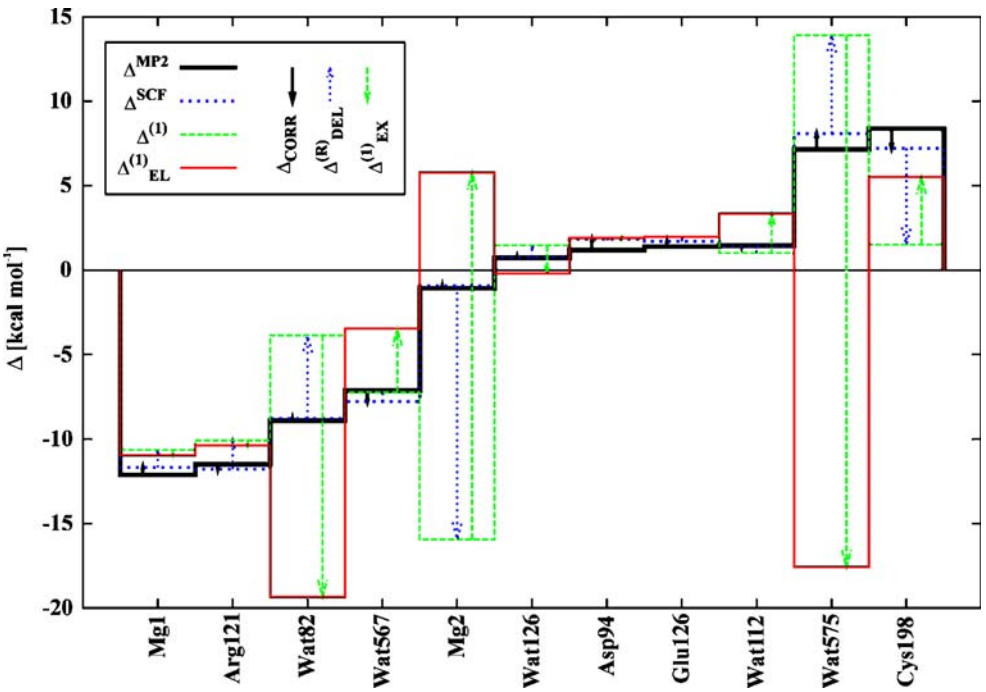

Fig. 5 The components of differential product stabilization with respect to transition state (DPS,TS) energy (kcal mol^{-1}). For each residue, the product stabilization energy (relative to transition state) is given at subseqent levels of theory. *Vertical arrows* show the mutual cancellation of correlation, delocalization, and exchange corrections to the MP2 interaction energy

Table 7 DPS,S energy (kcal mol^{-1}) at various levels of theory. Magnesium ions together with water molecules comprising their solvation sphere were considered as single residues. Similar treatment was also employed in case of Asp94, Arg121 residues

Residue	$\Delta_{EL}^{(1)}$	$\Delta^{(1)}$	Δ^{SCF}	Δ^{MP2}
Mg2:Wat	−21.96	−38.00	−32.16	−31.67
Glu126	−3.98	−3.97	−4.19	−4.06
Asp94:Arg121	−0.98	2.36	2.62	2.55
Cys198	0.39	2.89	3.27	3.07
Mg1:Wat	−17.47	16.99	9.50	7.29
Sum	−44.00	−19.73	−20.96	−22.81
R[a]	0.60	0.98	1.00	1.00

[a] Correlation coefficient—applies to the relationship between results at a particular level of theory and MP2 results

product relative to substrate. This observation applies to Arg121 either considered separately (Table 6) or as a part of Asp94:Arg121 cluster (Table 7). In this case, many-body effects turned out to be negligible—the sum of pairwise interactions is almost equal to the overall result obtained for the Asp94:Arg121 complex. However, in the case of solvated magnesium ions the non-additivity of interaction energy is significant. The latter can be seen not only when considering the DPS,S effects but also for DPS,TS and DTSS results. Interestingly, analysis of the contribution of particular solvated magnesium ions to differential stabilization of product relative to both transition state and substrate confirms the involvement of Mg1 in the preferential binding of transition state and substrate (with respect to product), whereas Mg2 seems to stabilize the product to a large extent. Compared to DTSS results, the correlation between electrostatic and reference MP2 interaction energy is surprisingly low—in the case of DPS,S, with all residues treated separately, there is no correlation at all (Table 6). Presumably, differential exchange effects are also required for the overall relative binding of products to be described accurately.

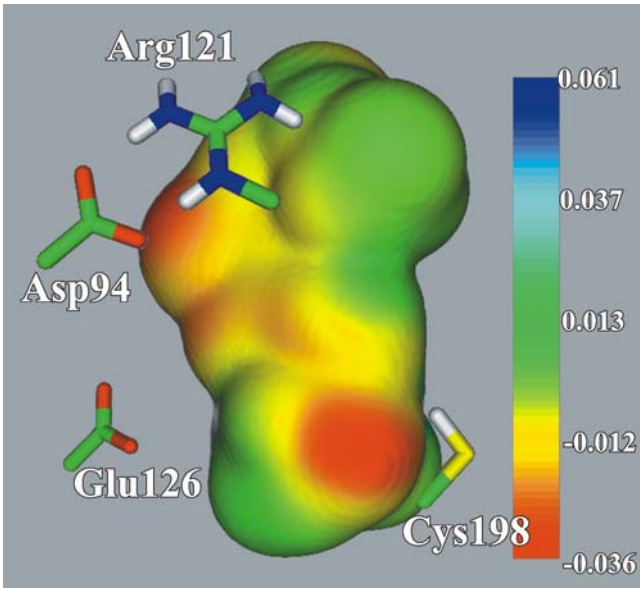

Fig. 7 Catalytic fields for the ThiK-catalyzed reaction juxtaposed with the positions of active site residues in a model system. Magnesium ions are considered as part of the transition state/reactants. The surface of constant electronic density is colored according to the differential electrostatic potential of transition state with respect to reactants. The sign of the differential potential is inverted to reflect the electrostatic properties of a complementary molecular environment. *Red* (*green*) color denotes regions where a negative (positive) charge would be optimal for catalytic activity

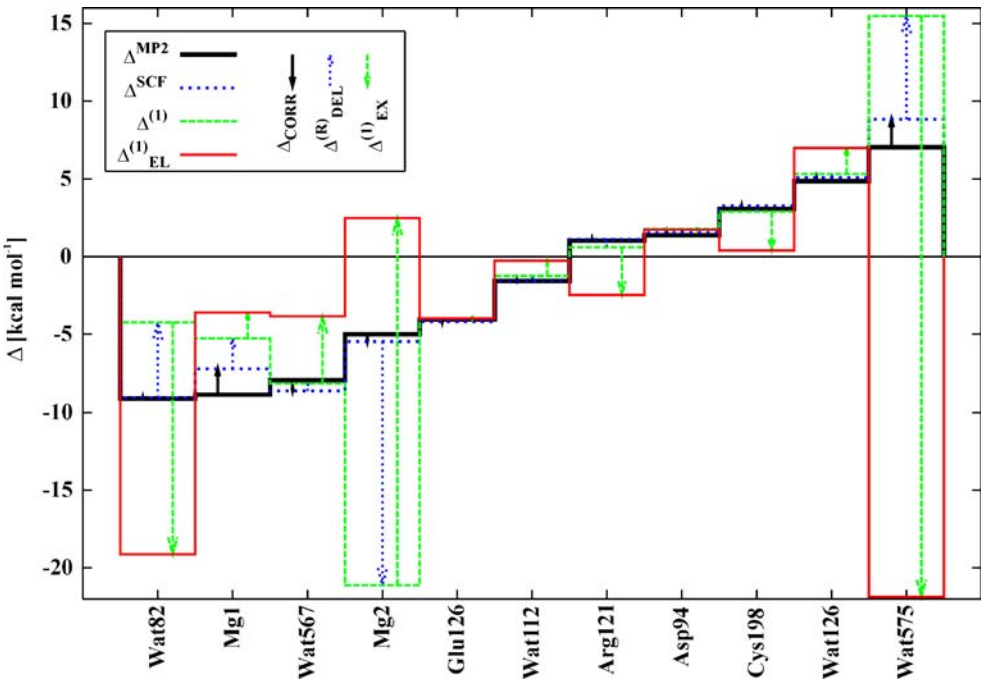

Fig. 6 The components of differential product stabilization with respect to substrate (DPS, S) energy (kcal mol^{-1}). For each residue, the product stabilization energy (relative to substrates) is given at subsequent levels of theory. *Vertical arrows* show the mutual cancellation of correlation, delocalization, and exchange corrections to the MP2 interaction energy

Optimal catalytic environment

Catalytic fields represent a hypothetical optimal molecular environment with electrostatic properties adjusted to enhance the rate of a given reaction (i.e., acting as a catalyst). Following the DTSS concept [26] one can consider the differential electrostatic potential of the transition state relative to the reactants (Fig. 7) to derive the electrostatic characteristics of an ideal catalyst that would promote a reaction by lowering the activation energy barrier. Notably, only a knowledge of the transition state and reactant structures is assumed, i.e., no prior knowledge of the catalytic environment is required. Figure 7 illustrates the catalytic field for the phosphoryl transfer reaction catalyzed by ThiK. The corresponding arrangement of ThiK active site residues is also presented. Examination of differential electrostatic potential reveals a pronounced change in charge distribution when going from reactants to the transition state. This indicates a legitimate need for this type of analysis to be performed as a part of the catalyst design process. Moreover, the evident agreement between electrostatic interaction energy and the reference MP2 results (correlation coefficient =0.88, see Table 2) further justifies the approximations applied in catalytic field derivation.

As anticipated by the catalytic field, the presence of a negative charge in the red-colored region would favor catalysis. One of these areas is already occupied by the negatively charged Asp94, while the other is located close to the neutral Cys198 residue. However, the experimental substitution of cysteine for the negatively charged aspartate residue results in increased catalytic activity [4], in perfect agreement with catalytic field predictions. Finally, the position of the Arg121 residue can also be matched to the green-colored region, showing the optimal influence of a positive charge.

Conclusions

The results presented in this report can be summarized as follows:

- A phosphoryl transfer mechanism consistent with experimental evidence was modelled using an ONIOM(B3LYP:PM3) approach according to an S_N2-like mechanism. The latter involves a nucleophilic attack of the thiazole hydroxyl group on the phosphorus atom followed by a single transition state with the hydroxyl proton already transferred to the γ-phosphate oxygen atom. No direct involvement of residue Cys198 was confirmed.
- For the structures obtained in the previous step, the enzyme–S/TS/P interaction energies were calculated at the MP2 level of theory and further decomposed into well-defined terms to reveal both the role of particular residues in enzyme catalytic activity as well as the physical nature of the observed effects. Residues Glu126 and Cys198 residues were found to be particularly important for both differential transition state stabilization and product release, while Arg121 appears to exert the opposite influence (except for differential product stabilization with respect to substrate). Assuming that product stabilization relative to substrate binding is more important from the point of view of product release rate, Arg121 could possibly augment the latter process.
- The magnesium ion Mg1 seems to play a role in product release, whereas Mg2 is involved in catalysis due to its contribution to activation energy barrier lowering.
- Electrostatic interaction energy is generally a dominant contribution of residues displaying catalytic activity for the forward reaction.
- Analysis of electronic charge redistribution along the reaction pathway allows the ideal catalytic environment to be derived from the first principles of quantum mechanics. Such an optimal molecular environment can then be compared with the evolutionarily conserved amino acid residues to identify its crucial components.
- In agreement with experimental data, catalytic fields for ThiK predict increased catalytic activity upon Cys198Asp mutation.

Acknowledgments This work is funded by the British–Polish Young Scientists Programme. The authors are also grateful for financial support from Wrocław University of Technology and Jackson State University subcontract #W912HZ-04-2-0002. Dr. Borys Szefczyk is acknowledged for the software for visualization of catalytic fields. Calculations were performed in Wrocław (WCSS) and Poznań (PCSS) Centers for Supercomputing and Networking as well as the Interdisciplinary Centre for Mathematical and Computational Modeling (ICM) in Warsaw.

References

1. Cheek S, Zhang H, Grishin NV (2002) J Mol Biol 320:855–881
2. Adams JA (2001) Chem Rev 101:2271–2290
3. Bork P, Sander C, Valencia A (1993) Prot Sci 2:31–40
4. Campobasso N, Mathews II, Begley TP, Ealick SE (2000) Biochemistry 39:7868–7877
5. Sigrell JA, Cameron AD, Jones TA, Mowbray SL (1998) Structure 6:183–193
6. Mathews II, Erion MD, Ealick SE (1998) Biochemistry 37:15607–15620
7. Li MH, Kwok F, Chang WR, Lau CK, Zhang JP, Lo SCL, Jiang T, Liang DC (2002) J Biol Chem 277:46385–46390
8. Matte A, Tari LW, Delbaere LTJ (1998) Structure 6:413–419
9. Becke AD (1993) J Chem Phys 98:5648–5652

10. Lee CT, Yang WT, Parr RG (1988) Phys Rev B 37:785–789
11. Stewart JJP (1989) J Comput Chem 10:209–220
12. Maseras F, Morokuma K (1995) J Comput Chem 16:1170–1179
13. Frisch MJ, Trucks GW, Schlegel HB, Scuseria GE, Robb MA, Cheeseman JR, Montgomery JR, Vreven T, Kudin KN, Burant JC, Millam JM, Iyengar SS, Tomasi J, Barone V, Mennucci B, Cossi M, Scalmani G, Rega N, Petersson GA, Nakatsuji H, Hada M, Ehara M, Toyota K, Fukuda R, Hasegawa J, Ishida M, Nakajima T, Honda Y, Kitao O, Nakai H, Klene M, Li X, Knox JE, Hratchian HP, Cross JB, Adamo C, Jaramillo J, Gomperts R, Stratmann RE, Yazyev O, Austin AJ, Cammi R, Pomelli C, Ochterski JW, Ayala PY, Morokuma K, Voth GA, Salvador P, Dannenberg JJ, Zakrzewski VG, Dapprich S, Daniels AD, Strain MC, Farkas O, Malick DK, Rabuck AD, Raghavachari K, Foresman JB, Ortiz JV, Cui Q, Baboul AG, Clifford S, Cioslowski J, Stefanov BB, Liu G, Liashenko A, Piskorz P, Komaromi I, Martin RL, Fox DJ, Keith T, Al-Laham MA, Peng CY, Nanayakkara A, Challacombe M, Gill PMW, Johnson B, Chen W, Wong MW, Gonzalez C, Pople JA (2004) Gaussian 03. Gaussian Inc, Wallingford CT
14. Dyguda E, Szefczyk B, Sokalski WA (2004) Int J Mol Sci 5:141–153
15. Bairoch A, Apweiler R, Wu CH, Barker WC, Boeckmann B, Ferro S, Gasteiger E, Huang H, Lopez R, Magrane M, Martin MJ, Natale DA, O'Donovan C, Redaschi N, Yeh LS (2005) Nucleic Acids Res 33:D154–D159
16. Thompson JD, Higgins DG, Gibson TJ (1994) Nucleic Acids Res 22:4673–4680
17. Gouet P, Courcelle E, Stuart DI, Metoz F (1999) Bioinformatics 15:305–308
18. Akola J, Jones RO (2003) J Phys Chem B 107:11774–11783
19. Diaz N, Field MJ (2004) J Am Chem Soc 126:529–542
20. Cheng Y, Zhang Y, McCammon JA (2005) J Am Chem Soc 127:1553–1562
21. Szefczyk B, Mulholland AJ, Ranaghan KE, Sokalski WA (2004) J Am Chem Soc 126:16148–16159
22. Dyguda E, Grembecka J, Sokalski WA, Leszczyński J (2005) J Am Chem Soc 127:1658–1659
23. Sokalski WA, Roszak S, Pecul K (1988) Chem Phys Lett 153:153–159
24. Boys FS, Bernardi D (1970) Mol Phys 19:553–566
25. Schmidt MW, Baldridge KK, Boatz JA, Elbert ST, Gordon MS, Jensen JH, Koseki S, Matsunaga N, Nguyen KA, Su SJ, Windus TL, Dupuis M, Montgomery JA (1993) J Comput Chem 14:1347–1363
26. Sokalski WA (1985) J Mol Catalysis 30:395–410
27. Cleland WW, Hengge AC (2006) Chem Rev 106:3252–3278
28. Brooks BR, Bruccoleri RD, Olafson BO, States DJ, Swaminathan S, Karplus M (1983) J Comput Chem 4:187–217
29. MacKerell AD Jr, Bashford D, Bellott M, Dunbrack RL Jr, Evanseck JD, Field MJ, Fischer S, Gao J, Guo H, Ha S, Joseph-McCarthy D, Kuchnir L, Kuczera K, Lau FTK, Mattos C, Michnick S, Ngo T, Nguyen DT, Prodhom B, Reiher WE III, Roux B, Schlenkrich M, Smith JC, Stote R, Straub J, Watanabe M, Wiorkiewicz-Kuczera J, Yin D, Karplus M (1998) J Phys Chem B 102:3586–3616
30. Grzywa R, Dyguda-Kazimierowicz E, Sieńczyk M, Feliks M, Sokalski WA, Oleksyszyn J (2007) J Mol Mod 13: DOI 10.1007/s00894-007-0193-8
31. Mildvan AS (1997) Proteins 29:401–416
32. Herberg FW, Doyle ML, Cox S, Taylor SS (1999) Biochemistry 38:6352–6360